Energy & Environmental Science

COMMUNICATION

A high thermoelectric figure of merit $ZT > 1$ in Ba heavily doped BiCuSeO oxyselenides†

Jing Li,[ab] Jiehe Sui,[*ab] Yanling Pei,[c] Celine Barreteau,[d] David Berardan,[d] Nita Dragoe,[d] Wei Cai,[ab] Jiaqing He[*e] and Li-Dong Zhao‡[*d]

A high ZT value of ~1.1 at 923 K in the BiCuSeO system is achieved *via* heavily doping with Ba and refining grain sizes (200–400 nm), which is higher than any thermoelectric oxide. Excellent thermal and chemical stabilities up to 923 K and high thermoelectric performance confirm that the BiCuSeO system is promising for thermoelectric power generation applications.

The thermoelectric (TE) energy conversion technology, which can be used to convert wasted heat into electricity, has received much attention in the past decade. The efficiency of TE devices is characterized by the dimensionless figure of merit, $ZT = (S^2\sigma/\kappa)T$, where S, σ, κ, and T are the Seebeck coefficient, the electrical conductivity, the thermal conductivity, and the absolute temperature, respectively. Until now, several classes of bulk materials with high ZT values have been discovered,[1,2] including nanostructured BiSbTe alloys,[3] filled skutterudites,[4] zinc antimonide,[5] $AgPb_{18+x}SbTe_{20}$,[6] Tl doped $PbTe$[7] or $(AgSbTe_2)_{1-x}(GeTe)_x$ alloys,[8] but they lack thermal and chemical stabilities in air. Therefore, TE oxides are expected to play an important role in extensive applications for waste heat recovery, on the basis of their potential advantage over heavy metallic alloys of chemical and thermal robustness. To date, several families of oxides have been developed as promising TE materials. Typical TE oxides include $Ca_{2.8}Ag_{0.15}Lu_{0.05}Co_4O_{9+\delta}$ ($\kappa \sim 1.4$ W m^{-1} K^{-1}, $ZT \sim 0.61$ at 1118 K),[9] $Sr_{0.9}La_{0.1}TiO_{3-\delta}$ ($\kappa \sim 3.0$ W m^{-1} K^{-1}, $ZT \sim 0.21$ at

750 K),[10] $In_{1.8}Ge_{0.2}O_3$ ($\kappa \sim 2.0$ W m^{-1} K^{-1}, $ZT \sim 0.46$ at 1273 K),[11] $Ca_{0.9}Yb_{0.1}MnO_3$ ($\kappa \sim 1.6$ W m^{-1} K^{-1}, $ZT \sim 0.16$ at 1000 K),[12] and $Zn_{0.96}Al_{0.02}Ga_{0.02}O$ ($\kappa \sim 5.0$ W m^{-1} K^{-1}, $ZT \sim 0.65$ at 1247 K).[13] These ZT values still remain significantly lower than those of some metallic alloys, which can be ascribed to either moderate electrical conductivity or high thermal conductivity depending on the families. Even though the ZT values can be enhanced to unity in cobalt oxide-based materials by single crystal growth, these materials are unstable against humidity.[14,15] Recently, we have reported the promising TE properties of a quaternary oxyselenide, BiCuSeO, which exhibits an intrinsically very low thermal conductivity (~0.40 W m^{-1} K^{-1} at 923 K).[16,17] High ZT values of 0.76 at 873 K,[16] 0.81 at 923 K[17a] and 0.90 at 923 K[17c] can be achieved by optimizing the electrical conductivity through Sr doping, Cu vacancies and Ca doping, respectively. The main features of the BiCuSeO system can be summarized as:[16,17] the crystal structure constituted by $(Cu_2Se_2)^{2-}$ layers alternately stacked with $(Bi_2O_2)^{2+}$ layers along the c axis of the tetragonal cell;[16–18] a moderate effective mass ($m^* \sim 0.60m_o$); low hole mobility (2–20 cm^{-2} V^{-1} s^{-1}); a large Gruneisen parameter ($\gamma \sim 1.5$) and a low Young's modulus ($E \sim 76.5$ GPa). These features lead to a moderate power factor coupled to a very low thermal conductivity. In this work, we show that Ba^{2+} doping on the Bi^{3+} site can be used to optimize the charge carrier concentrations, which results in an improved power factor, and meanwhile the grain size can be refined using a ball milling process in order to reduce the lattice thermal conductivity contribution without diminishing the electrical conductivity. A ZT value of 1.1 is reached at 923 K for $Bi_{0.875}Ba_{0.125}CuSeO$ with carrier concentrations as high as 1.1×10^{21} cm^{-3}, which is the highest value ever reported for oxygen containing materials.[9–15]

Samples with the chemical composition $Bi_{1-x}Ba_xCuSeO$ ($x = 0$, 0.025, 0.05, 0.075, 0.1, 0.125, and 0.15) were synthesized by a two-step solid state reaction route. A stoichiometric mixture of Bi_2O_3 (4 N), Bi (3 N), Cu (3 N), Se (5 N) and BaO (3 N) powders was prepared by a ball milling process and then the mixed powders were cold pressed using a graphite die and heated at 573 K for 8 h and 1023 K for 24 h in vacuum in a hot pressing sinter. The obtained bulk materials were crushed into powders and then ball milled at 250 rpm for 8 h in a planetary ball mill. Finally, the obtained powders were sintered by a spark plasma sintering system (Sumimoto SPS1050, Japan) under the axial compressive stress of 50 MPa in vacuum at 973 K for 6 min, resulting in a disk-shaped sample of Ø 20 × 7 mm. The sample preparation processes including weighing raw materials and ball

[a]*School of Materials Science and Engineering, Harbin Institute of Technology, Harbin 150001, China. E-mail: suijiehe@hit.edu.cn*

[b]*National Key Laboratory Precision Hot Processing of Metals, School of Materials Science and Engineering, Harbin Institute of Technology, Harbin 150001, China*

[c]*School of Materials Science and Engineering, Beihang University, Beijing 100191, China*

[d]*LEMHE, ICMMO (CNRS UMR 8182), Univ. Paris Sud, Orsay F91405, France. E-mail: lidong-zhao@northwestern.edu*

[e]*Frontier Institute of Science and Technology (FIST), Xi'an Jiaotong University, Xi'an 710054, China. E-mail: hejiaqing@mail.xjtu.edu.cn*

† Electronic supplementary information (ESI) available: Typical samples (bar and coin) used in this study (Fig. S1); temperature dependence of heat capacity, thermal diffusivity, Lorenz number, and electronic thermal conductivity (Fig. S2) for $Bi_{1-x}Ba_xCuSeO$ samples; and thermoelectric properties of the samples before and after annealing treatments (Fig. S3). See DOI: 10.1039/c2ee22622g

‡ L. -D. Zhao is presently in the Department of Chemistry, Northwestern University, Evanston, Illinois 60208, USA.

milling were carried out in air. The obtained samples were sealed inside an evacuated quartz tube with a pressure of $\sim 10^{-4}$ torr and annealed at 923 K for 7 days to evaluate their thermal stability. The obtained SPS processed pellets were cut along the radial direction of the disk sample into bars with dimensions of about 18 mm × 3 mm × 3 mm that were used for simultaneous measurement of the Seebeck coefficient and the electrical conductivity using an Ulvac Riko ZEM-2 instrument (ZEM-2, ULVAC-RIKO, Japan) under a helium atmosphere from room temperature to 923 K. Heating and cooling cycles gave repeatable electrical properties, verifying the thermal stability. Electrical properties obtained from different slices cut from the same pellets were similar, attesting to the homogeneity of the samples. The uncertainty of the Seebeck coefficient and electrical conductivity measurements is 5%. High density SPSed pellets were cut as shown in Fig. S1 (ESI†) and the thermal and electrical transport properties were measured in the same direction. The SPSed pellets were polished into coins of $\varnothing \sim 6$ mm and 1–2 mm thickness for thermal diffusivity measurements. The samples were coated with a thin layer of graphite to minimize errors from the emissivity of the material. The thermal conductivity was calculated from $\kappa = DC_p\rho$, where the thermal diffusivity coefficient (D) in the range from room temperature to 923 K was measured using the laser flash diffusivity method in a Netzsch LFA427 (NETZSCH, LFA427, Germany), the thermal diffusivity data were analyzed using a Cowan model with pulse correction and heating and cooling cycles gave reproducible values for each sample. The specific heat capacity (C_p) was determined by differential scanning calorimetry (NETZSCH DSC 404C Germany). The density (ρ) was determined by using the dimensions and mass of the sample, which was then reconfirmed using the Archimedes method. Thermal diffusivities obtained for different slices from the same pellet are also similar. The uncertainty of the thermal conductivity is estimated to be within 8%, considering the uncertainties for D, C_p and ρ. The combined uncertainty for all measurements involved in the calculation of ZT is less than 15%. The Hall coefficients, R_H, of the samples were measured at room temperature using a physical properties measurement system (PPMS-9T, Quantum Design Inc, USA), and a magnetic field of 2 T and an electrical current of 30 mA were applied. The carrier concentration (n_H) was calculated by $n_H = 1/eR_H$, where e is the electronic charge. The carrier mobility (μ) was calculated by $\mu = \sigma R_H$, where σ is the electrical conductivity. Thermogravimetric analysis was performed by using a METTLER TGA/SDTA851e differential thermal analyzer under an Ar–air atmosphere in the temperature range from room temperature to 923 K with a rate of 5 K min^{-1}. *X-ray diffraction and electron microscopy*: the phase structure was analyzed by X-ray diffraction (XRD, CuKα, Bruker D8, Germany). Scanning electron microscopy (SEM) studies were performed using a Hitachi S-3400N VP-SEM equipped with an Oxford detector for energy dispersive X-ray spectroscopy (EDS). The samples used for SEM and EDS were the same coins used for thermal diffusivity measurements, and they were polished using a suspension of 50 nm Al$_2$O$_3$ particles. Transmission electron microscopy (TEM) investigations were carried out using a JEOL 2100F microscope operated at 200 kV. The thin TEM specimens were prepared by conventional standard methods. The procedures include cutting, grinding, dimpling, polishing and Ar-ion milling on a liquid nitrogen cooling state subsequently.

Fig. 1(a) shows the powder XRD patterns of Bi$_{1-x}$Ba$_x$CuSeO, all the major Bragg peaks show an excellent match to the simulation of BiCuSeO (PDF#82-0464) and can be indexed to the ZrSiCuAs type
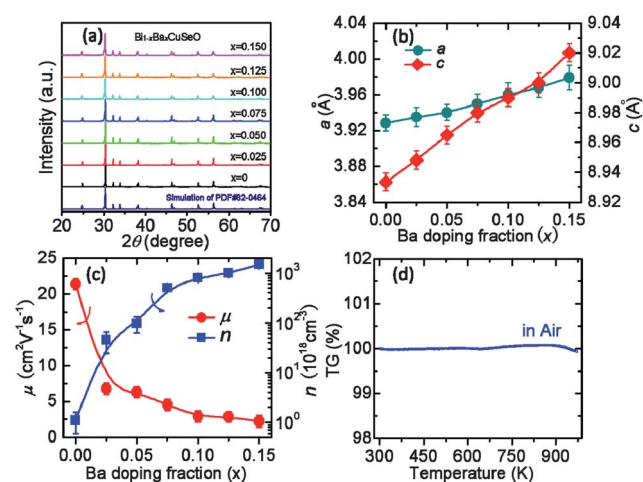

Fig. 1 (a) Powder XRD patterns for Bi$_{1-x}$Ba$_x$CuSeO samples. (b) Lattice parameters as a function of Ba doping fraction for the Bi$_{1-x}$Ba$_x$CuSeO sample. (c) Room temperature carrier mobility and carrier concentration as a function of Ba doping content. (d) Thermogravimetric analysis in air atmosphere from room temperature to 923 K for the BiCuSeO sample.

structure. The lattice parameters as a function of Ba doping content are shown in Fig. 1(b). Both a and c values increase with the increasing Ba content, which is related to the radius of Ba^{2+} ions (1.34 Å), which is larger than that of Bi^{3+} ions (0.96 Å). The Hall carrier concentration (n_H) at 300 K increases rapidly from 1.1 × 10^{18} cm^{-3} for BiCuSeO to 8.0 × 10^{20} cm^{-3} for $x = 0.1$ Ba doped sample, and further increases to 1.5 × 10^{21} cm^{-3} for $x = 0.15$ Ba doping, as shown in Fig. 1(c). Collectively, the lattice parameters and carrier concentration variations indicate that Ba^{2+} was successfully incorporated into the BiCuSeO lattice. Typical thermogravimetric analysis (TGA) for BiCuSeO under air atmosphere shows that the sample is thermally and chemically stable up to 923 K with no measurable weight loss or gain, as shown in Fig. 1(d). It is noteworthy that thermal and chemical stabilities of BiCuSeO outperform NaCo$_2$O$_4$ oxide,[15] which is the highest performance TE oxide reported so far, and that of most TE metallic alloys.[1–8]

The sample of Bi$_{0.875}$Ba$_{0.125}$CuSeO was investigated by TEM. Fig. 2(a) shows a typical low magnification TEM image with grain sizes ranging from 200 nm to 400 nm. The inset of Fig. 2(a) shows an
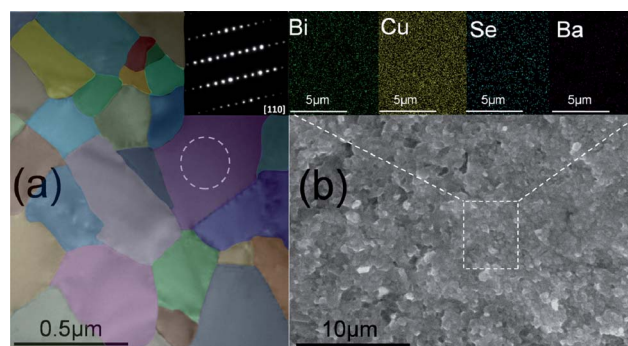

Fig. 2 (a) Low magnification TEM image of Bi$_{0.875}$Ba$_{0.125}$CuSeO. (b) SEM fractography for Bi$_{0.875}$Ba$_{0.125}$CuSeO, the inset shows element distributions determined by EDX.

electron diffraction pattern with the selected area aperture including only one grain marked as a circle in Fig. 2(a), which is consistent with the layer structure feature of BiCuSeO. The electron diffraction pattern can be easily indexed as [110] direction. No split Bragg spots can be observed, which confirms that Ba^{2+} was successfully incorporated into the BiCuSeO lattice. SEM fractography indicates a highly dense sample with uniform grain sizes, Fig. 2(b). The composition of the $Bi_{0.875}Ba_{0.125}CuSeO$ was examined using elemental mapping and SEM, indicating that actual Ba doping levels are similar to nominal ones. The elemental distributions determined by energy dispersive X-ray spectroscopy (EDX) indicate that all the elements are homogeneously distributed throughout the sample, as shown in the inset of Fig. 2(b).

Fig. 3 shows the temperature dependence of the TE properties for $Bi_{1-x}Ba_xCuSeO$ samples. $Bi_{1-x}Ba_xCuSeO$ with $0 \leq x \leq 0.15$ are identified according to the measured Hall carrier concentrations ($n_H = 1/eR_H$) at room temperature, as listed in Table 1. As shown in Fig. 3(a), BiCuSeO exhibits low electrical conductivity values over the entire temperature range and a semiconducting behavior. Upon Ba doping, the electrical transport changes to a metal-like behavior and shows a significant increase with increasing Ba doping, from $\sim$1.12 S cm^{-1} (BiCuSeO) to $\sim$535 S cm^{-1} ($Bi_{0.85}Ba_{0.15}CuSeO$) at 300 K, which is consistent with the strongly increased charge carrier concentration. Indeed, similarly to the LaFeAsO superconductors,[19] the enhanced electrical conductivity of $Bi_{1-x}Ba_xCuSeO$ can be explained by carriers introduced into the conductive $(Cu_2Se_2)^{2-}$ layers in response to the introduction of negative charge into the insulating $(Bi_2O_2)^{2+}$ layers through substitution of Bi^{3+} by Ba^{2+}.

Table 1 A list of samples, carrier concentrations and Seebeck coefficients at room temperature

Label	Composition	n_H (10^{21} cm^{-3})	S (μV K^{-1})
1E18	BiCuSeO	0.001	349
4E19	$Bi_{0.975}Ba_{0.025}CuSeO$	0.045	232
1E20	$Bi_{0.95}Ba_{0.05}CuSeO$	0.098	165
5E20	$Bi_{0.925}Ba_{0.075}CuSeO$	0.5	139
8E20	$Bi_{0.90}Ba_{0.10}CuSeO$	0.8	105
1E21	$Bi_{0.875}Ba_{0.125}CuSeO$	1.1	81
2E21	$Bi_{0.85}Ba_{0.15}CuSeO$	1.5	64

The Ba doping also has a significant effect on the Seebeck coefficient value, as shown in Fig. 3(b). The positive Seebeck coefficient indicates a p-type electrical transport behavior. The Seebeck coefficient values of BiCuSeO are large, from +353 μV K^{-1} at 300 K to +420 μV K^{-1} at 923 K, and decrease with increasing Ba doping fractions, down to +69 μV K^{-1} at 300 K and +167 μV K^{-1} at 923 K for the $Bi_{0.85}Ba_{0.15}CuSeO$ sample, which is consistent with the increased carrier concentration. The relatively large Seebeck coefficients for BiCuSeO should be related to the moderate effective mass ($m^* = 0.60m_o$),[17c] which is larger than those of PbTe ($0.24m_o$)[20] and PbS ($0.40m_o$)[21] with rock salt structure. The combined electrical conductivity and positive temperature-dependent Seebeck coefficient result in a maximum power factor that reaches $\sim$6.33 μW cm^{-1} K^{-2} for the $Bi_{0.875}Ba_{0.125}CuSeO$ sample at 923 K, Fig. 3(c), which shows that the optimum power factor in the BiCuSeO system is reached for heavily doped levels.

Fig. 3(d) shows the total thermal conductivity κ_{tot} as a function of temperature for $Bi_{1-x}Ba_xCuSeO$ samples. The κ_{tot} of BiCuSeO decreases with increasing temperature from 0.54 W m^{-1} K^{-1} at 300 K to 0.34 W m^{-1} K^{-1} at 923 K (heat capacity and thermal diffusivity data can be found in Fig. S2†). These values over the entire measuring temperature range are much lower than 0.89 W m^{-1} K^{-1} at 300 K and 0.45 W m^{-1} K^{-1} at 923 K for the BiCuSeO sample prepared by cold pressing followed by solid state sintering,[17c] which mainly results from refining the particle sizes (200–400 nm) by the ball milling process included in this report.[17b] These κ_{tot} values are much lower than those of high-performance TE materials,[1,2] even lower than that of nanostructured Bi–Sb–Te.[3] κ_{tot} increases with increasing carrier concentration (Ba doping fractions), which is caused by the electronic heat transport contribution, but still maintains very low over the entire measuring temperature range, e.g., 0.78 W m^{-1} K^{-1} at 300 K and 0.52 W m^{-1} K^{-1} at 923 K for the 2E21 sample ($x = 0.15$ Ba doping). In a general case, a decreased grain size leads to a decrease of the lattice thermal conductivity due to the increased scattering of phonons at the interfaces, but also to a decreased electrical conductivity which partly mitigates the improvement of ZT. However, BiCuSeO based materials exhibit low carrier mobilities in the optimum doping range, which corresponds to a small carrier mean free path, much lower than the grain size. Therefore, a moderate decrease of the grain size, from several μm to 200–400 nm, can be successfully used to scatter the medium to long wavelength phonons and to decrease the lattice thermal conductivity while keeping the electrical conductivity unchanged.

Indeed, Fig. 3(e) shows the lattice thermal conductivity κ_{lat} as a function of temperature for $Bi_{1-x}Ba_xCuSeO$ samples with different carrier concentrations. Generally, κ_{lat} can be estimated by directly
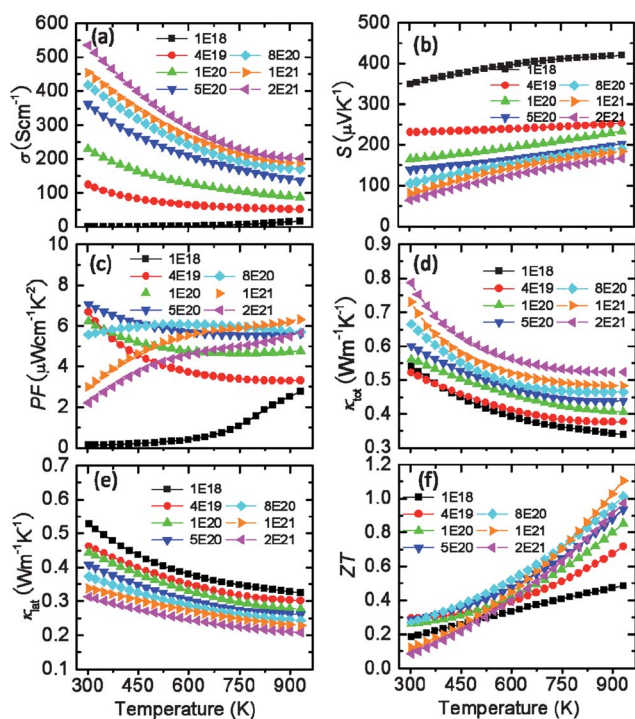

Fig. 3 Thermoelectric properties of $Bi_{1-x}Ba_xCuSeO$ as a function of temperature. (a) Electrical conductivity. (b) Seebeck coefficient. (c) Power factor. (d) Total thermal conductivity. (e) Lattice thermal conductivity. (f) Figure of merit ZT.

subtracting the electronic thermal conductivity κ_{ele} from the total thermal conductivity κ_{tot}. κ_{ele} is related to the electrical conductivity σ through the Wiedemann–Franz relation, $\kappa_{ele} = L\sigma T$, where L is the Lorenz number which can be obtained in detail as described in reports,[20,21] Lorenz number and κ_{ele} for $Bi_{1-x}Ba_xCuSeO$ are shown in Fig. S2.† BiCuSeO has a very low κ_{lat} of 0.52 W m^{-1} K^{-1} at 300 K and 0.32 W m^{-1} K^{-1} at 923 K, which are much lower than those of PbTe-based TE materials.[6,7,20] The value of 0.52 W m^{-1} K^{-1} is close to the minimum value of $\kappa_{lat,min} = 0.47$ W m^{-1} K^{-1} at 300 K that is estimated by the minimum phonon mean path l to be the interatomic distance,[22,23] which is estimated to be ~3.0 Å for BiCuSeO.[17c] The possible origins that cause the intrinsically low thermal conductivity of BiCuSeO are the weak chemical bonds (Young's modulus, $E \sim 76.5$ GPa) or the strong anharmonicity of the bonding arrangement (Gruneisen parameter, $\gamma \sim 1.5$).[17b,17c] Other possible reasons include the layered structure since phonons can be confined and scattered layer interfaces,[22,24] presence of heavy elements,[1,2] etc. All these features can be shortly summarized as involving heavy atoms with 'soft' bonding, which can meet the requirements for a lower thermal conductivity selection as suggested by Clarke.[25] In Ba doped BiCuSeO the κ_{lat} is presumably reduced by point defect scattering through Ba doping, as it has been observed in Sr or Ca doped BiCuSeO.[16,17c] Indeed, a clear trend can be readily seen where the κ_{lat} decreases with increasing carrier concentration (Ba doping fraction). Namely, the κ_{lat} at 300 K decreases from 0.52 W m^{-1} K^{-1} for BiCuSeO to 0.31 W m^{-1} K^{-1} for the 2E21 sample. The further reduction in the lattice thermal conductivity of Ba doped BiCuSeO can be explained by the point defects on the basis of the Callaway model,[17c] in which the point defect scattering in a solid solution system originates from both the mass differences (the mass difference is ~71.65 a.u. (Ba ~ 137.33, Bi ~ 208.98)) and the interatomic coupling force differences derived from the size difference (strain field fluctuations, the size difference is ~0.38 Å ($Ba^{2+} \sim 1.34$ Å, $Bi^{3+} \sim 0.96$ Å)) between the impurity atom and the host lattice.[26,27]

By using the electrical and thermal transport properties, the ZT value is calculated as shown in Fig. 3(f). ZT shows an increasing trend with temperature, the maximum ZT value of 1.1 is achieved at 923 K for the 1E21 sample ($x = 0.125$ Ba doping), this value is higher than that of 0.76 for $Bi_{0.925}Sr_{0.075}CuSeO$[16] at 873 K, 0.81 at 923 K for $BiCu_{0.975}SeO$[17a] and 0.90 at 923 K for $Bi_{0.925}Ca_{0.075}CuSeO$.[17c] The present ZT value of 1.1 is higher than that of any TE oxide reported so far[9-15] and is close to the values observed in most of the TE metallic alloys:[1,2] SiGe, CoSb$_3$ Mg$_2$Si, etc. Therefore, the high TE performance of Ba doped BiCuSeO, which originates from the intrinsically low thermal conductivity and optimized carrier concentration, makes these materials robust candidates for medium temperature TE applications.

Finally, one may suggest that the presence of nano-grain sizes in the BiCuSeO system makes the materials unstable. To check the thermal stability of these high-performance samples at elevated temperature we annealed several samples of $Bi_{1-x}Ba_xCuSeO$ ($x = 0.05, 0.125$ and 0.15) at 923 K for 7 days. After the annealing treatment, the ZT values at 923 K almost show no changes, Fig. S3,† absence of any sign of degradation suggests potential power generation applications for waste-heat recovery in the temperature range up to 923 K. Actually, besides annealing treatments, the thermal stability can also be evidenced from the fact that the heating and cooling cycles in the TE properties measurement gave repeatable TE properties up to 923 K.

Acknowledgements

References

1 (a) M. G. Kanatzidis, Chem. Mater., 2010, 22, 648–659; (b) J. R. Sootsman, D.-Y. Chung and M. G. Kanatzidis, Angew. Chem., Int. Ed., 2009, 48, 8616–86139; (c) M. G. Kanatzidis, Semicond. Semimetals, 2000, 69, 51–100; (d) C. J. Vineis, A. Shakouri, A. Majumdar and M. G. Kanatzidis, Adv. Mater., 2010, 22, 3970–3980.

2 (a) J.-F. Li, W. S. Liu, L.-D. Zhao and M. Zhou, NPG Asia Mater., 2010, 2, 152–158; (b) J. G. Snyder and E. S. Toberer, Nat. Mater., 2008, 7, 105–114; (c) M. S. Dresselhuas, G. Chen, M. Tang, R. Yang, H. Lee, D. Wang, Z. Ren, J. Fleurial and P. Gogna, Nat. Mater., 2007, 19, 1043–1053; (d) M. Zebarjadi, K. Esfarjani, M. S. Dresselhaus, Z. F. Ren and G. Chen, Energy Environ. Sci., 2012, 5, 5147–5162.

3 B. Poudel, Q. Hao, Y. Ma, Y. Lan, A. Minnich, B. Yu, X. Yan, D. Wang, A. Muto, D. Vashaee, X. Chen, J. Liu, M. S. Dresselhaus, G. Chen and Z. F. Ren, Science, 2008, 320, 634–638.

4 A. Harnwunggmoung, K. Kurosaki, H. Muta and S. Yamanaka, Appl. Phys. Lett., 2010, 96, 202107(1–3).

5 T. Caillat, J. Fleurial and A. Borshchevsk, J. Phys. Chem. Solids, 1997, 58, 1119–1125.

6 K. F. Hsu, S. Loo, F. Guo, W. Chen, J. S. Dyck, C. Uher, T. Hogan, E. K. Polychroniadis and M. G. Kanatzidis, Science, 2004, 303, 818–821.

7 J. P. Heremans, V. Jovovic, E. S. Toberer, A. Saramat, K. Kurosaki, A. Charoenphakdee, S. Yamanaka and G. J. Snyder, Science, 2008, 321, 554–557.

8 B. A. Cook, M. J. Kramer, X. Wei, J. L. Harringa and E. M. Levin, J. Appl. Phys., 2007, 101, 053715(1–6).

9 N. V. Nong, N. Pryds, S. Linderoth and M. Ohtaki, Adv. Mater., 2011, 23, 2484–2490.

10 J. Liu, C. L. Wang, W. B. Su, H. C. Wang, P. Zheng, J. C. Li, J. L. Zhang and L. M. Mei, Appl. Phys. Lett., 2009, 95, 162110(1–3).

11 D. Berardan, E. Guilmeau, A. Maignan and B. Raveau, Solid State Commun., 2008, 146, 97–101.

12 D. Flahaut, T. Mihara, R. Funahashi, N. Nabeshima, K. Lee, H. Ohta and K. Koumoto, J. Appl. Phys., 2006, 100, 084911(1–4).

13 M. Ohtaki, K. Araki and K. Yamamoto, J. Electron. Mater., 2009, 38, 1234–1238.

14 M. Shikano and R. Funahashi, Appl. Phys. Lett., 2003, 82, 1851(1–3).

15 (a) I. Terasaki, Y. Sasago and K. Uchinokura, Phys. Rev. B: Condens. Matter, 1997, 56, 12685–12687; (b) K. Fujita, T. Mochida and K. Nakamura, Jpn. J. Appl. Phys., 2001, 40, 4644–4647.

16 L.-D. Zhao, D. Berardan, Y. L. Pei, C. Byl, L. Pinsard-Gaudart and N. Dragoe, Appl. Phys. Lett., 2010, 97, 092110(1–3).

17 (a) Y. Liu, L.-D. Zhao, Y. C. Liu, J. L. Lan, W. Xu, F. Li, B. P. Zhang, D. Berardan, N. Dragoe, Y. H. Lin, C. W. Nan, J. F. Li and H. M. Zhu, J. Am. Chem. Soc., 2011, 133, 20112–20115; (b) F. Li, J.-F. Li, L.-D. Zhao, K. Xiang, Y. Liu, B.-P. Zhang, Y.-H. Lin, C.-W. Nan and H. M. Zhu, Energy Environ. Sci., 2012, 5, 7188–7195; (c) Y.-L. Pei, F. Li, J.-F. Li, Q.-J. Liu, W. Pan, C. Barreteau, D. Berardan, N. Dragoe, J. Q. He, L.-D. Zhao, 2012, submitted; (d) C. Barreteau, D. Berardan, E. Amzallag, L.-D. Zhao, N. Dragoe, 2012, submitted; (e) D. Berardan, L.-D. Zhao, C. Barreteau and N. Dragoe, Phys. Status Solidi A, 2012, DOI: 10.1002/pssa.201228341.

18 (a) H. Hiramatsu, H. Yanagi, T. Kamiya, K. Ueda, M. Hirano and H. Hosono, Chem. Mater., 2008, 20, 326–334; (b) E. S. Stampler, W. C. Sheets, M. I. Bertoni, W. Prellier, T. O. Mason and K. R. Poeppelmeier, Inorg. Chem., 2010, 47, 10009–10016.

19 (a) P. Quebe, L. J. Terbuchte and W. Jeitschko, J. Alloys Compd., 2000, 302, 70–74; (b) Y. Kamihara, H. Hiramatsu, M. Hirano,

8546 | Energy Environ. Sci., 2012, 5, 8543–8547

This journal is © The Royal Society of Chemistry 2012

R. Kawamura, H. Yanagi, T. Kamiya and H. Hosono, *J. Am. Chem. Soc.*, 2008, **130**, 3296–3297.

20 (*a*) I. I. Ravich, B. A. Efimova, I. A. Smirnov, *Semiconducting Lead Chalcogenides*, Plenum Press, New York, 1970; (*b*) S. N. Girard, J. Q. He, X. Y. Zhou, D. Shoemaker, C. M. Jaworski, C. Uher, V. P. Dravid, J. P. Heremans and M. G. Kanatzidis, *J. Am. Chem. Soc.*, 2011, **133**, 16588–16597.

21 (*a*) L.-D. Zhao, S.-H. Lo, J. Q. He, H. Li, K. Biswas, J. Androulakis, C.-I. Wu, T. P. Hogan, D.-Y. Chung, V. P. Dravid and M. G. Kanatzidis, *J. Am. Chem. Soc.*, 2011, **133**, 20476–20487; (*b*) L.-D. Zhao, J. Q. He, C.-I. Wu, T. P. Hogan, X. Y. Zhou, C. Uher, V. P. Dravid and M. G. Kanatzidis, *J. Am. Chem. Soc.*, 2012, **134**, 7902–7912; (*c*) S. Johnsen, J. Q. He, J. Androulakis, V. P. Dravid, I. Todorov, D.-Y. Chung and M. G. Kanatzidis, *J. Am. Chem. Soc.*, 2011, **133**, 3460–3470.

22 (*a*) R. Venkatasubramanian, E. Siivola, T. Colpitts and B. O'Quinn, *Nature*, 2001, **413**, 597–602; (*b*) L. D. Hicks and M. S. Dresselhaus, *Phys. Rev. B: Condens. Matter*, 1993, **47**, 12727–12731.

23 (*a*) D. T. Morelli, V. Jovovic and J. P. Heremans, *Phys. Rev. Lett.*, 2008, **101**, 035901–035904; (*b*) T. Zhou, B. Lenoir, M. Colin, A. Dauscher, R. A. R. A. Orabi, P. Gougeon, M. Potel and E. Guilmeau, *Appl. Phys. Lett.*, 2011, **98**, 162106(1–3); (*c*) J. Y. Cho, X. Shi, J. R. Salvador, G. P. Meisner, J. Yang, H. Wang, A. A. Wereszczak, X. Zhou and C. Uher, *Phys. Rev. B: Condens. Matter Mater. Phys.*, 2011, **84**, 085207(1–9).

24 J. Q. He, S. N. Girard, J. C. Zheng, L.-D. Zhao, M. G. Kanatzidis and V. P. Dravid, *Adv. Mater.*, 2012, DOI: 10.1002/adma.201201565.

25 D. R. Clarke, *Surf. Coat. Technol.*, 2003, **163**, 67.

26 C. L. Wan, W. Pan, Q. Xu, Y. X. Qin, J. D. Wang, Z. X. Qu and M. H. Fang, *Phys. Rev. B: Condens. Matter Mater. Phys.*, 2006, **74**, 144109(1–9).

27 (*a*) J. Callayway and H. C. Von Baeyer, *Phys. Rev.*, 1960, **120**, 1149–1154; (*b*) T. K. Dey and K. D. Chaudhuri, *J. Low Temp. Phys.*, 1976, **23**, 419–426; (*c*) J. Yang, G. P. Meisner and L. D. Chen, *Appl. Phys. Lett.*, 2004, **85**, 1140(1–3).